Controlled Airspace Boundary Detection

Michael Cahill

A dissertation submitted to the University of Dublin, in partial fulfillment of the requirements for the degree of Master of Science in Computer Science

2010

Declaration

I declare that the work described in this dissertation is, except where otherwise stated, entirely my own work and has not been submitted as an exercise for a degree at this or any other university.

Signed: ____________________

Michael Cahill

13 September 2010

Permission to lend and/or copy

Acknowledgements

I would like to thank my supervisor Eamonn O'Nuallain for his help and assistance throughout this project. I would like to thank Dr. David Abrahamson whose idea Airspace Boundary Detection is for allowing me to work on this project and for his assistance. Finally I would like to thank the ubicom class for a fun and enjoyable year.

Michael Cahill

University of Dublin, Trinity College
2010

Abstract

This dissertation outlines an attempt to solve the problem of controlled airspace infringements. An infringement occurs when an aircraft enters controlled airspace without permission. This happens most frequently to light aircraft whose pilots have made a navigation error. Such infringements can have serious consequences such as midair collisions.

The following chapters outline the design of a proof of concept hardware device which detects a controlled airspace and alerts a pilot to its presence. The device is designed to detect existing radio navigation beacons and signal a warning when the range to a beacon drops below a certain threshold.

The final chapter draws conclusions from the research and outlines possibilities for further development of the system.

Contents

List of Figures

List of Tables

Chapter 1

Introduction

1.1 Introduction

This dissertation is an attempt to design a warning system which would alert pilots of light aircraft that they are approaching controlled airspace. Currently, controlled airspace is marked on maps and pilots must plot their courses accordingly. Sometimes, though, the pilots of light aircraft can lose their way and stray into the controlled airspace of an airport [1, 2]. This can lead to dangerous situations where a light aircraft crosses the paths of large commercial jet aircraft with the consequent risk of a collision.

The problem of controlled airspace infringement has grown over time for two reasons. Growth in the commercial aviation sector is the main reason. It leads to the reclassification of more airspace as controlled airspace when major airports expand their capacity. The second reason is growth in the number of light aircraft in use.

In the period from 1996 to 2006, there were an average of 389 airspace infringements per year in the UK [3]. In the Republic of Ireland, figures for airspace infringements are reported per 100,000 aircraft movements. From 2006 to 2009 an average of 5.75 infringements per 100,000 movements occurred [1]. Given that there were an average of 304,000 movements each year, then at least 15 airspace infringements happened each year [4].

Each infringement event brings with it (i) the risk of a mid air collision and (ii) an economic impact through delays caused by runway closures while the infringing aircraft exits the controlled airspace.

In this project two approaches to solving the problem of controlled airspace infringment were considered. The initial approach consisted of simulating an aircraft and an airspace boundary marking beacon using MICAz motes.

The second approach involved building a detector capable of detecting the signal from the VHF Omnidirectional Range navigation system present at all major airports. The signal strength of this navigation system could then be used to decide if an aircraft was approaching too close to the airport.

1.2 Research Goals

The goal of this project is to produce a proof of concept version of a Controlled Airspace Boundary Detector for light aircraft. The two main properties the detector must have are:

- The detector must provide adequate warning to the pilot of an aircraft when it detects the presence of a signal indicating that there is controlled airspace ahead.
- The detector must be simple, contain very few components and need very little power.

The first requirement is the most important requirement for both a proof of concept device and a commercially produced device. Simplicity is a requirement of all devices on aircraft to avoid adding to a pilot's workload. The device needs to have a small component count and need little power so that it can be fitted to aircraft with even the most stringent weight and power limits.

1.3 Structure

This chapter has covered the motivations for the project and the research goals.

Chapter 2 gives an overview of the state of the art. It includes an overview of the definitions of various types of controlled airspace and an overview of the transmission technologies used by the aviation sector. It also describes the basics of antennas and discusses the hardware and software used in the project.

Chapter 3 covers the initial prototype research using MICAz motes and TinyOS.

Chapter 4 describes in detail the demonstration system built using dedicated hardware. It gives a detailed explanation of each component of the detector and an overview of the completed detector.

Chapter 5 discusses tuning the assembled system and the results of testing the system.

Chapter 6 draws conclusions and discusses some possible future work which would improve the detector.

The appendices contain code listings etc.

Chapter 2

Background

This chapter presents an overview of the regulations, technologies and physics which underlie the design and implementation of a proof-of-concept Controlled Airspace Boundary Detector. It begins with some definitions related to controlled airspace and the transmission technologies used at airports. Then the motes used in the early prototyping stage are discussed in detail along with their communication protocol, (ZigBee) and the software running on them, (TinyOS and NesC). The final sections of the chapter provide a brief overview of the Global Positioning System (GPS) and the physics of antennas and circuits.

2.1 Controlled Airspace

Controlled airspace is divided up into a number of classes, A to G [5], by the International Civil Aviation Authority (ICAO) [6]. Each country has definitions for their controlled airspace which closely follow these international guidelines. In Ireland all airspace falls into one of the three classes A, C or G [7].

The airspace around an airport is broken into three zones. At the center is the Control Zone (CTR). In Ireland this is generally a cylinder with a radius of 15 nautical miles and a height from the ground of 2,500 feet [8]. Above the Control Zone, and extending beyond it, is the Control Area (CTA). The control area extends from a specified lower altitude to a specified upper altitude. The CTA can be any shape but is often a rectangular box aligned with the runways at the airport. In Dublin airport for example the upper limit is 24,000 feet [9]. In Ireland the CTR and CTA zones correspond to class C of the ICAO airspace designations [5,7]. The final zones are called Air Traffic Service (ATS) routes. These are routes of controlled airspace, usually between airports [9]. ATS routes define the path between airports and include specifications such as the minimum safe altitude on the route.

There are a number of other types of airspace which are less common, including *danger* area, *prohibited* area and *restricted* area [5]. These special areas surround various military or civilian sites of a high security nature, such as nuclear power plants and military bases.

2.2 Transmission Technologies

There are a large number of electromagnetic transmission technologies used at all modern airports. These include communications radios at Very High Frequency (VHF) and High Frequency (HF), navigation aids such as instrument landing systems (ILS), and monitoring systems such as radar.

Airports use a large number of HF and VHF bands for communication with aircraft. HF radio reserved for use by airports in Ireland is at frequencies between 2MHz and 10MHz, and VHF radio at frequencies between 108MHz and 140MHz [10, 11]. These frequency bands are divided between communication, navigation and monitoring uses.

Radar is used at airports for determining the velocity and position of aircraft. All airports have both primary and secondary radar systems. Primary radar works by detecting reflected pulses of radio waves. It is used to calculate the position and velocity of the aircraft which the beam intercepts. Secondary radar systems interrogate the aircraft they detect using a pulsed signal. All large aircraft carry a transponder which responds to the pulses with an identification code [12]. Secondary radar transmits at a frequency of 1030MHz and replies are sent by aircraft at 1090MHz [10, 13, 14].

Navigation aids at airports come in two forms: short range systems such as Instrument Landing System (ILS) and long range systems such as Very High Frequency Omni directional Range (VOR).

VOR provides navigation beacons along the ATS routes between airports [15]. VOR works by encoding the azimuth (angle to a station) in the phase relationship between a variable and a reference signal. The variable signal rotates at 1800 r.p.m. [16], and its phase varies in phase with its azimuth angle. The reference signal phase is constant at all azimuth angles. Bearings calculated using the system are relative to magnetic north [16]. VOR uses frequencies between 108 and 118MHz [16, 17], and has a typical range of 100 nautical miles [18].

Distance measuring equipment (DME) is usually co-located with VOR. It allows aircraft to calculate their distance from the ground station by timing the interval between sending out a series of pulses and receiving a corresponding sequence of pulses in reply [17].

2.3 MICAz Motes

In this section, the MICAz wireless sensor systems (developed by Crossbow [19], and now owned and produced by MEMSIC [20]) are described in detail. Areas described include the antenna, the radio chip and the micro controller. Figure 2.1 shows a picture of a typical MICAz mote.

By default, a MICAz mote is equipped with a $\frac{\lambda}{4}$ antenna [22,23]. The antenna is a simple monopole, (described in Section 2.7) and takes the form of an insulated length of wire. In [23], Su et al. present the results of an investigation of the propagation characteristics of MICAz motes. Their measurements of the radiation pattern of the mote antenna show that it

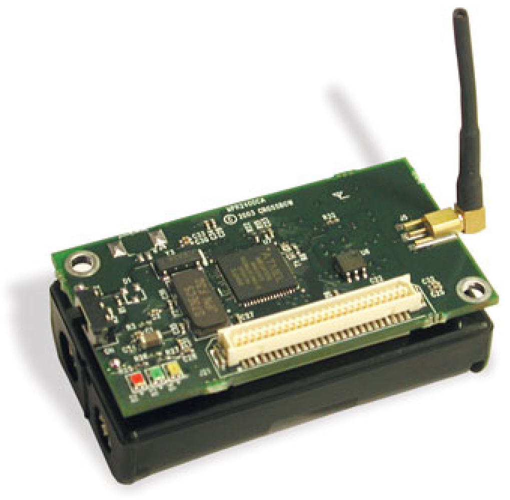

Figure 2.1: MICAz mote. *(Image reproduced from MICAz user manual [21])*

has an almost perfect monopole radiation pattern [23]. They found a slight distortion (< 5 dBm) in the radiation pattern due to the antenna being attached at one end of the mote as opposed to being centrally positioned on the device.

MICAz motes use a cc2420 RF transceiver built by Texas Instruments [21]. The cc2420 chip implements the IEEE 802.15.4 standard [24], and can transmit data at more than ten times the rate of earlier chips such as the cc1000 (used in the MICA2 mote) [25]. The chip has a number of useful features, including programmable transmission power, separate transmit and receive first in first out (FIFO) registers, and two different measures of link quality, Received Signal Strength Indicator (RSSI) and Link Quality Indication (LQI). The chip is configured via a Serial Peripheral Interface (SPI) bus. The RSSI can be continuously read from the chip using the SPI bus [22]. The value of the RSSI can be used to determine if the chip is detecting a signal without decoding any packets [22]. The chip has a typical sensitivity of -95 dBm [22], which is much greater than the -85 dBm required by the IEEE 802.15.4 standard [24]. The RSSI's total range is -100 dBm to 0 dBm, with an accuracy of ± 6 dBm. The value in the RSSI register of the cc2420 is averaged over eight symbol periods [22]. A symbol period is defined as the time taken to send a unit of information such as a byte.

The microcontroller on the MICAz is an ATmega128 8-bit RISC processor manufactured by ATMEL [26]. The ATmega128 runs the TinyOS operating system, which will be described in the next section. The microcontroller is connected to the cc2420 radio chip via an SPI bus. This allows an application running in TinyOS on the microcontroller to interact directly with the radio system.

The mote's capabilities can be expanded by adding plug-in sensor boards [27]. Sensor boards can be used to add a large number of additional functions to a mote. These functions can include accelerometers, sound and light sensors, and also a Global Positioning System (GPS) receiver. Figure 2.2 shows a picture of the MTS420cc sensorboard used in this project. The sensorboard is described in more detail in the next chapter.

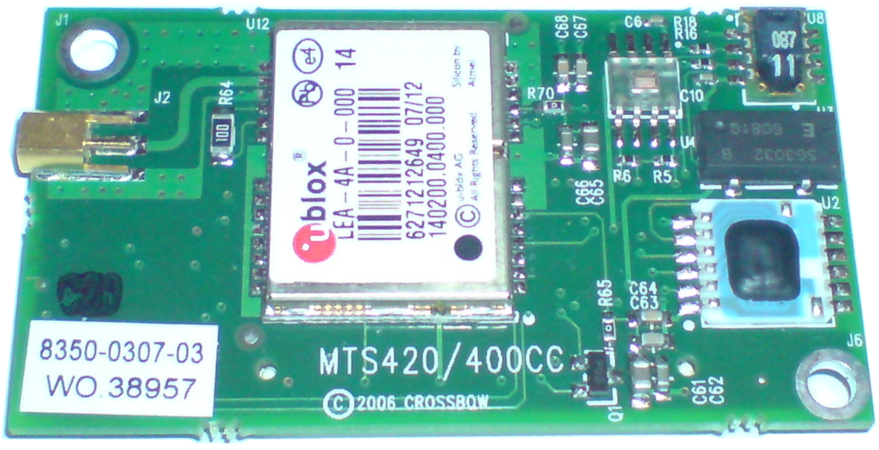
Figure 2.2: MTS420cc Sensor Board

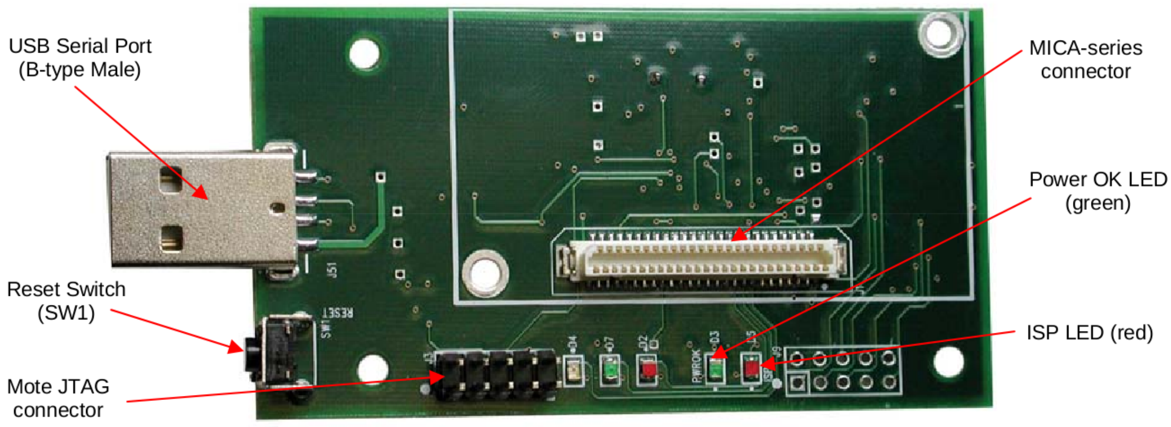

Figure 2.3: MIB520CB Programming Board *(Image reproduced from MICAz user manual [21])*

Programming of the MICAz motes is done using the MIB520CB USB Interface Board described in the MPR/MIB manual [21]. In the Linux system used throughout this project, the programming board is recognised as a USB (Universal Serial Bus) device. It is assigned an identifier such as **/dev/ttyUSB2** where the number depends on how many USB devices are connected to the computer.

2.4 ZigBee and IEEE 802.15.4

IEEE 802.15.4 is a wireless communication standard for personal area networks. It defines the physical and medium access control layers. ZigBee is an implementation of two transport layers, (network (NWK) and application (APL)) on top of IEEE 802.15.4 [28, 29]. ZigBee has the same relationship to IEEE 802.15.4 as WiFi has to IEEE 802.11. Figure 2.5 illustrates how ZigBee and IEEE 802.15.4 fit together.

The physical layer of IEEE 802.15.4 supports three different frequency bands, including the 2.4GHz industrial, scientific and medical (ISM) band [24]. The PHY layer uses Direct

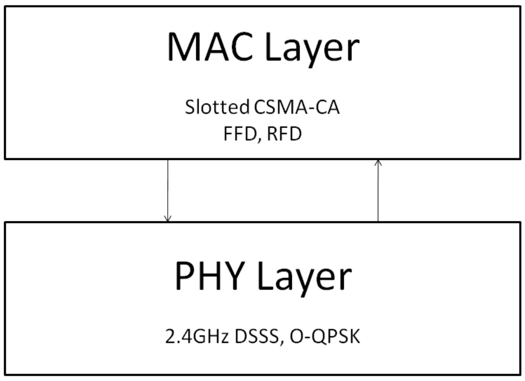

Figure 2.4: Structure of IEEE 802.15.4

Sequence Spread Spectrum (DSSS) as an access mode, with Offset Quadrature Phase Shift Keying (O-QPSK) as its modulation [28]. The PHY layer is illustrated in Figure 2.4.

The MAC layer of IEEE 802.15.4 supports a slotted carrier sense multiple access - collision avoidance (CSMA-CA) protocol. Two types of device are possible - full function devices (FFD) and reduced function devices (RFD). The difference between an FFD and RFD is that an FFD can act as a network controller whereas a RFD can only be an end device [28, 29]. The MAC layer is illustrated in Figure 2.4.

The ZigBee network layer is designed to provide support for multi-hop routing [29] across networks with an arbitrary arrangement of FFD and RFD devices. ZigBee's application layer is designed to provide support for the development and deployment of distributed programs [28]. ZigBee specifies three different device types an end device, a router and a coordinator. These are illustrated in figure 2.5. These three device types can be used to create a multitude of network topologies [28]. The ZigBee end device is equivalent to an RFD. A router or coordinator node is an FFD at the lower layer.

The application layer of ZigBee specifies a number of parts - ZigBee Device Objects (ZDO), the Application Sub Layer (APS) and Application Objects (APO) [28]. The APOs are user-defined modules which add functionality to a particular system. The APOs on a particular deployment use the network service and device discovery interface provided by a device's ZDO to perform their programmed functions [28], [29]. The APS talks to the network layer of the ZigBee deployment.

2.5 TinyOS and NesC

TinyOS is an operating system designed for use on embedded systems [30]. TinyOS is written in the NesC language. NesC stands for Networked Embedded Systems C [31]. NesC is a variant of the C programming language. It allows developers to create modules which encapsulate basic functionality such as blinking the Light Emitting Diodes (LEDs) on a mote. The TinyOS system is available for a number of platforms including Microsoft Windows and Linux [30]. In this project, TinyOS was installed on a computer running Ubuntu Linux 10.04.

The goal of NesC is to allow a modular style of programming while using much of the

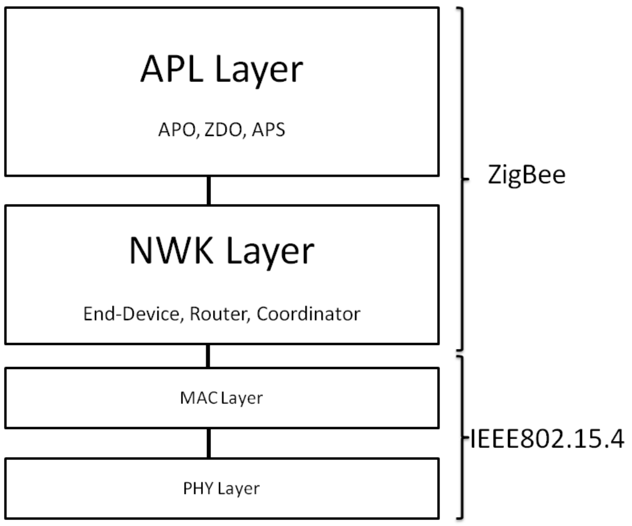

Figure 2.5: ZigBee Structure

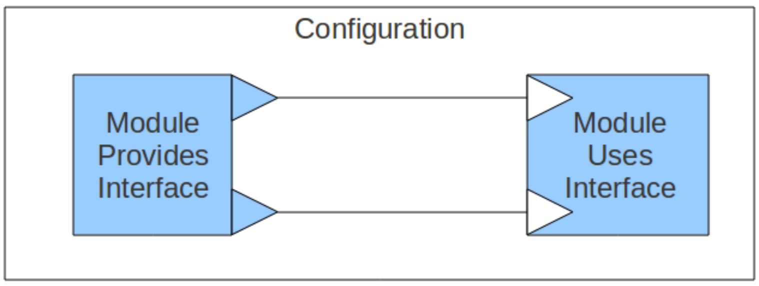

Figure 2.6: NesC, Modules and Configuration

syntax of the C programming language. All functionality in TinyOS is provided in the form of components. Components come in two forms - modules and configurations. Modules provide interfaces consisting of events and commands. To call the commands provided by an interface a module must implement all of the events provided by the interface. Configurations are a special type of component which connect the modules using an interface to the modules providing the interface. These connections are called *wiring* [31] and allow compile time checking of all possible code execution paths. To provide an interface, a module must implement the commands defined by an interface and signal the events. Figure 2.6 shows an overview of NesC. A module providing two interfaces is represented with triangles pointing out of a rectangle. A module using an interface is represented with a triangle pointing into the rectangle. The lines joining the user to the provider represent the wiring done in the configuration. Appendix A shows a listing of the code from the Blink tutorial [32] which will be discussed further in chapter 3.

When the modules of an application are wired together with the necessary hardware components provided by TinyOS to form an application the result compiles to a single executable. This executable is then loaded to the hardware, usually a mote, using a customized GNU toolchain provided with the TinyOS system [32].

The TinyOS system provides a task queue to which application programmers can post tasks with the *post* command. Tasks in the TinyOS system cannot preempt each other; however, a hardware interrupt can preempt an executing task [33]. Only one instance of a task can exist on the task queue; however, once a task begins executing it is no longer part of the queue and can be reposted to the task queue. This behaviour allows a task to remain alive on a permanent basis.

2.6 Global Positioning System

The Global Positioning System is a satellite navigation system developed by the United States military in the 1960's and 70's [34]. It consists of a constellation of 24 satellites in orbit around the earth [35]. Each satellite in the constellation transmits signals containing a precise time generated by an atomic clock [34], along with information about the satellite's orbital parameters. Receivers on the ground including the GPS receiver on the MTS420cc sensor board, use the signals from at least 4 satellites to calculate their position and altitude [36].

The receiver calculates its own position by finding the intersection of 4 spheres defined by the received signals. The radius of the spheres is calculated as follows. Each signal contains the transmission time of the signal t_i where i is the number of the satellite, 1 to 4. t_r is the received time of the signal at the receiver. The radius of any sphere is given by $(t_r - t_i)c$ where c is the speed of light $(3 \times 10^8 ms^{-1})$. Two spheres will intersect at either a point or a circle. (The case of two spheres not intersecting is not relevant for the GPS system.) The third sphere calculated will intersect the point or circle intersection of the first two at a maximum of two points. Calculation of the fourth sphere allows the correct position from the 3-sphere calculation to be selected. This is usually the point closest to the earth's surface [36].

2.7 Antennas

At a fundamental level, an antenna is a device which converts electrical waves in a wire to radiating waves in free space. All electromagnetic phenomena are described by Maxwell's equations [37]. These fundamental laws basically state that only accelerating electric charges produce electromagnetic waves. The goal of all antenna design is to make the process of generating electromagnetic waves from accelerating electrons as efficient as possible.

There are a large number of antenna designs, the most basic type being a *center-fed* dipole antenna [38]. The simplest center fed dipole is made from two pieces of straight wire. Figure 2.7 illustrates a typical arrangement for a center fed dipole antenna. The signal generator is connected to the centre of the dipole and the electric fields in the two halves of the dipole add to produce a lobe shaped radiation pattern. In three dimensions it is seen that a dipole antenna produces a torus shaped radiation pattern [38]. The torus is in a plane perpendicular to the axis of the dipole as illustrated in Figure 2.8.

Other antenna types include *monopole* antennas, *parabolic dish* antennas, *loop* and *he-*

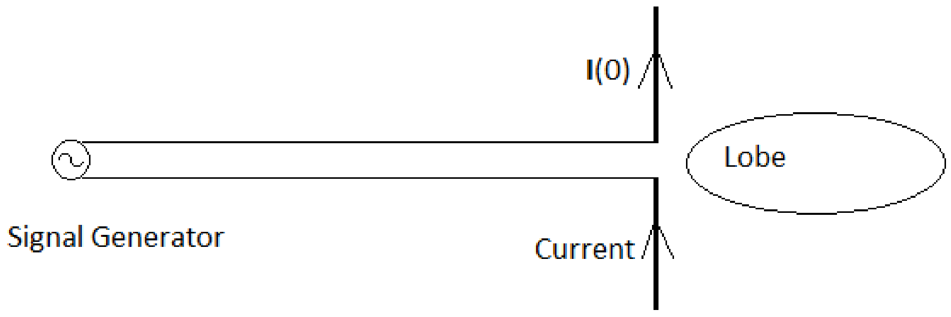

Figure 2.7: Dipole Antenna

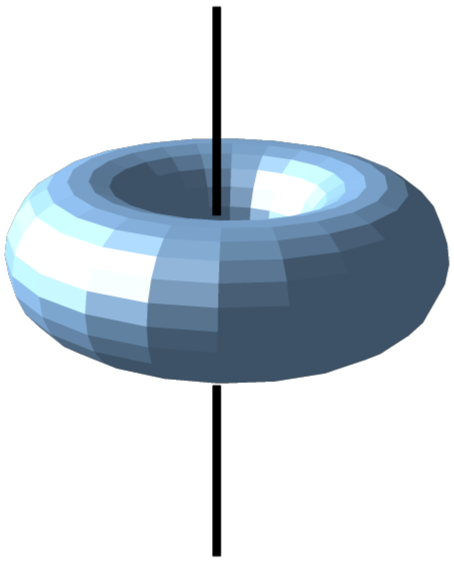

Figure 2.8: Dipole Radiation Pattern

lical antennas. *Horn* antennas are used for high frequency (> 1GHz) applications. *Patch* antennas, which are printed on circuit boards, are used where compact size is a requirement [38].

The Friis formula relates the power transmitted to the power received:

$$\frac{P_r}{P_t} = G_a G_b \left(\frac{\lambda}{4\pi r}\right)^2 \tag{2.1}$$

Where G_a, G_b are the gain of the transmitter and receiver, respectively, λ is the wavelength of the radiation, and r is the distance between transmitter and receiver. P_r and P_t are the received and transmitted powers, respectively.

The gain is related to the geometric shape of an antenna. This relationship is called the aperture of the antenna.

$$G = \frac{4\pi}{\lambda^2} A_e \tag{2.2}$$

Where A_e is the aperture of the antenna. The aperture is easy to visualize in the case of a dish antenna (it is simply the diameter), but is applicable to all types of antenna [38].

2.8 Review of basic circuit theory

This section presents a brief overview of some basic equations used in circuit calculations. These equations are used extensively in chapter 4 which covers the design of the final experimental system.

The most basic equation is Ohm's law, which states that the voltage (V) is equal to the current (I) flowing in a conductor times the resistance (R) [37].

$$V = IR \tag{2.3}$$

The power (P) produced in a conductor by a current I can be shown experimentally to obey the following law [37].

$$P = RI^2 \tag{2.4}$$

For solving problems involving complete circuits, Kirchoff's laws are indispensable. Kirchoff's first law states that current splits at a junction in a circuit and that the total current entering the junction must be equal to the total current leaving the junction. Kirchoff's voltage law states that in a closed loop the sum of the voltage drops must be equal to the voltage of the power supply.

A potential divider, which consists of a pair of resistors, can be used to obtain a lower voltage from a high voltage supply. Figure 2.9 shows a typical potential divider. The power supply is connected to $\mathrm{V_{in}}$ and the ground terminal. The output is measured between $\mathrm{V_{out}}$ and the ground terminal. The output voltage is calculated from the equation

$$V_{out} = \frac{R_2}{R_1 + R_2} V_{in} \tag{2.5}$$

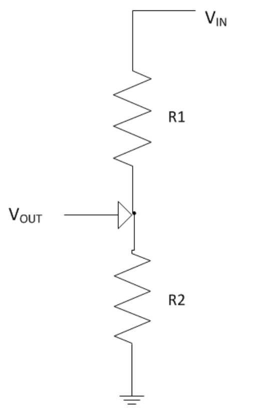

Figure 2.9: Potential Divider

Chapter 3

Mote Development

Initial work in this project was aimed at developing a mote based proof-of-concept Controlled Airspace Boundary Detector. To build a demonstration version using MICAz motes, a number of problems were identified which needed to be solved. Firstly, to simplify initial detection of a boundary marking signal, the RSSI value detected by the mote would have to monitored for significant changes. Secondly, the position and velocity of the mote representing the aircraft would have to be determined from the GPS sensor. Thirdly, the altitude of the mote would have to be determined either from the GPS sensor or from the barometric pressure sensor on the MTS420 sensor board [39]. This chapter describes all three of these areas in detail, and concludes with a discussion of the reasons for building the demonstration system described in chapter 4.

3.1 Reading the RSSI register

The RSSI (Received Signal Strength Indicator) register on the cc2420 stores an 8-bit value representing the average signal strength over the last eight symbol periods [22]. When the chip is initially powered on, the RSSI value is inconsistent until the first eight symbol periods have elapsed. No hardware level setup or configuration is required to activate the RSSI register. Figure 3.1 shows a graph of the RSSI value verses the Radio Frequency (RF) input power. The graph demonstrates that the relationship between the two is close to linear.

Initial work towards reading the RSSI register of the cc2420 chip using TinyOS consisted of reading the TinyOS tutorials, the TinyOS programming manual and the TinyOS Enhancement Proposals (TEPs) [31, 40, 41]. A number of useful features of the TinyOS system were identified as a result of this work. Firstly, a number of demonstration programs provided with the TinyOS system could be adapted for our work with little or no modification. These included the BaseStation application and the SendingMote application. Secondly, the presence of a debugging library and PC-based receiver program which uses it were identified. Finally, based on reading the tutorials, programming manual and TEP 126 (which describes the TinyOS cc2420 radio stack implementation), it became clear that the RSSI register should be accessed through the *CC2420ControlC* component.

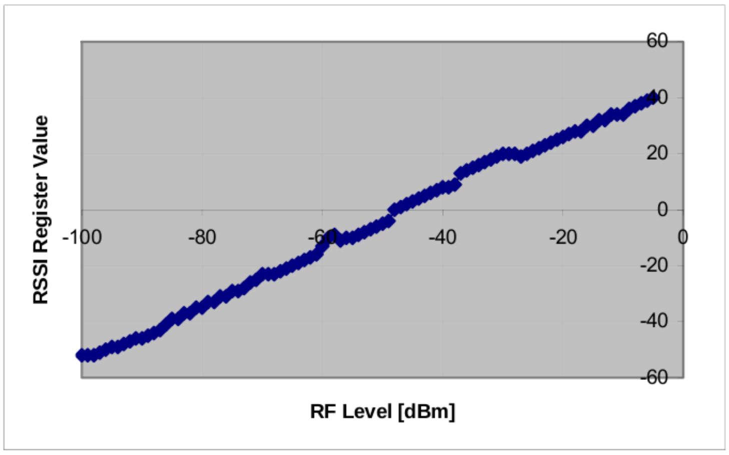

Figure 3.1: RSSI value vs RF Power *(Image reproduced from cc2420 manual [22])*

3.1.1 First attempt to read the RSSI register

The Blink demonstration application provided with the TinyOS system (See Appendix A.1 for the source code) was studied to gain familiarity with the NesC language and TinyOS. The application originally blinked the three LED's on the MICAz mote (see figure 2.1); the code shown in appendix A.1 has been reduced to blinking one LED for space-saving reasons. The application was successfully installed on a mote using the following commands

```
make micaz
make micaz reinstall mib520,/dev/ttyUSB0
```

which verified that the TinyOS system was correctly installed and configured as per the instructions in the tutorial [32].

The RSSI demo provided as part of the TinyOS system, and discussed in the RSSI demo tutorial [42], extracts the RSSI value from the headers of packets received by a mote. For the purposes of this project a simpler approach of directly reading the RSSI register was chosen. To achieve this, the ReadRSSI application listed in Appendix A.2 was created. It follows the instructions from the TinyOS programming manual, which lists the steps below as necessary for activating the cc2420 radio chip from TinyOS.

1. Turn on the voltage regulator
2. Acquire the SPI bus to the radio
3. Start the radio's oscillator by sending a command over the bus
4. Put the radio in RX (receive) mode

Reading of the RSSI register was done using the *read* interface which the *CC2420ControlC* component of the TinyOS radio stack implementation (see figure B.1), provides for the register.

The startup sequence of the radio is initiated in the *booted* event by a method call to start the radio's voltage regulator. The subsequent steps of the chain are initiated in the event handlers for the previous step's completion event. For example when control of the SPI bus passes to the application, the *resource-granted* event is signaled which kicks off the starting of the oscillator.

```
event void Resource.granted()
  {
    call Power.startOscillator();
  }
```

The final event in the chain is the *startOscillator* event which places the application in the *started* state.

```
async event void Power.startOscillatorDone()
  {
    call Fifo.enableFallingEdge();
    call Sfd.captureRisingEdge();
    call Power.rxOn();

    call Resource.release();

    //Change state to started
    atomic
    {
      state = STATE_STARTED;
    }
  }
```

When the application enters the *started* state, the event handler for the *timer-fired* event calls the *read* command on the RSSI register. This *read* command is split-phase, so it returns immediately, and the value of the RSSI register is returned by the system when it signals the *readDone* event.

```
event void Read.readDone(error_t result, uint16_t val)
  {
    if ( result == SUCCESS )
    {
      printf("\t\t%d\n", val);
    }
    else
    {
      printf("failed to read rssi\n");
    }
    printfflush();
  }
```

The *readDone* event sends the RSSI value to the PC over the serial line using the printf debugging library. The PC must have the PrintfClient java application (which is provided with the TinyOS system) running to receive the printed values [43].

Testing of the ReadRSSI application was performed by loading a second mote with the SendingMote demo program which is part of the RSSI tutorial [42]. The SendingMote application simply broadcasts an empty packet periodically. This empty packet should have been occasionally detected and shown as a high value in the RSSI values being printed on the PC screen. The result, however, was that the RSSI value would increase and then fail to be subsequently updated by the hardware.

Three potential causes were identified based on a careful reading of the cc2420 manual. The three potential causes identified are

- Address Recognition possibly leaving the SFD (start frame delimiter) pin in the wrong state.
- No receiver for the incoming packets.
- RX (Receive) buffer not flushed.

Each probable cause was investigated in succcession, but was eliminated without a positive result. Resetting the SFD pin had no effect, attaching a dummy receiver prevented any increase in the RSSI value. and flushing the RX buffer also had no effect.

3.1.2 Second attempt to read the RSSI register

Based on advice from another researcher and because of the unlikelihood of isolating the underlying bug within the time constraints of the project, a complete rewrite was performed. In the second version it was decided to use a high level component of the TinyOS radio stack ActiveMessageC to start the radio. See appendix A.3 for a complete listing of the code. The reading of the RSSI register was triggered every 50ms by a timer and was carried out in a similar fashion to the first version of the program, by using the ReadRSSI interface of the CC2420ControlC component.

Testing of this new version of the program revealed that it worked as expected (high values of RSSI when a packet was being received, and low values at all other times). The author suspects that the source of the error in the first version of the code was related to the handling of the SFD captured event. Extensive reading of the source code of the TinyOS radio stack did not, however, lead to a full understanding of the cause of the problem.

Appendix A.4 shows another version of the ReadRSSI application which uses a task to read the RSSI register. This minor rewrite of the code performs exactly the same as the timer-based version described in this section. This task-based version of the code would however be more readily extensible to incorporate other sensors such as the GPS sensor discussed in the next section.

3.2 GPS Driver

With the code for reading the RSSI working, attention was focused on getting the position of the mote from the GPS sensor on the MTS420 sensor board. The MTS420CC sensor board uses a uBlox LEA-4A GPS module [44]. The earlier CA and CB versions of the MTS420 board use a Leadtek GPS-9546 module. Examination of the TinyOS system showed that there was no driver supplied for the MTS420 sensor board. An online search located a driver for the CA version of the board, developed by the Rincon Corporation and available freely on the TinyOS repository [45,46].

3.2.1 Testing of the Leadtek driver

The Leadtek driver, which, as described above, was designed for earlier versions of MTS420 sensor boards, was tested on the CC version of the board. It failed to operate the uBlox GPS module. Testing was performed by running the TestNmeaParse application provided with the Leadtek driver on a mote with the MTS420 sensorboard and GPS antenna attached. During the test, a modified version of the BaseStation application was running on a mote connected to the PC. This BaseStation application was modified to allowing decoding of the GPS packets sent by the TestNmeaParse application on the first mote. The BaseStation code was modified in a number of ways. Firstly, the definition of the NMEA packets was added,

```
static nmea_gga_msg_t *gpsPkt; //Incoming gps data
```

then the *receive* event was modified to act only on the reception of GPS packets.

```
event message_t *RadioReceive.receive[am_id_t id](
message_t *msg,
    void *payload,
    uint8_t len) {
    if (len == sizeof(nmea_gga_msg_t)) {
      gpsPkt = (nmea_gga_msg_t *)payload;

      printf("lat %d %d %c",
        gpsPkt->latitude.degree, gpsPkt->latitude.minute,
        gpsPkt->latitude.direction);
      printf(" long %d %d %c",
        gpsPkt->longitude.degree, gpsPkt->longitude.minute,
        gpsPkt->longitude.direction);
      printf(" alt %d\n", gpsPkt->altitude);
      printfflush();
    }

    return msg;
}
```

Finally, the decoded data was forwarded to the PC using the printf debugging library discussed earlier in this chapter.

Based on a comparison of the manual for the older Leadtek module [47] and the uBlox module, it was discovered that both modules adhered to the NMEA 0183 standard for GPS communication [48]. Because of the common communication protocol, it was felt that a driver for the uBlox module could be built by reusing a large proportion of the Leadtek driver.

3.2.2 Creation of a uBlox GPS module driver

As a first step in the creation of the driver, a copy of the Leadtek driver files was created, and the name changes in table 3.1 were performed. Files which are used by the new driver but not changed are not listed in the table. Numerous small changes were required internally in each file. Modules using the files were updated to use the renamed files. Module and configuration names within the files were also adapted. For example,

```
configuration gps9546C {
```

becomes

```
configuration gpsUbloxLea4aC {
```

The next step in the driver development process was to examine the parts of the code where the hardware settings are specified, such as this segment (from Nmea.h [46])

```
enum {
  NMEA_START = 0x24,//$
  //NMEA_END1 = 0x0D,//CR
  NMEA_END = 0x0A,//LF -- NMEA 'sentence' terminator
  NMEA_DELIMETER = 0x2C,//','
  NMEA_CHECKSUM_DELIM = 0x2A,//'*'
  ASCII_PERIOD = 0x2E,//ASCII period '.'
  ASCII_ZERO = 0x30,//ASCII zero '0'
  ASCII_FIVE = 0x35,//ASCII five '5'
  ASCII_NINE = 0x39,//ASCII nine '9'
  ASCII_A = 0x41,//ASCII 'A'
  ASCII_G = 0x47,//ASCII 'G'
  ASCII_M = 0x4D,//ASCII 'M'
  ASCII_P = 0x50,//ASCII 'P'
};
```

and modify them to match the specifications mentioned in the uBlox manual [44]. In the case of the above segment the third line was uncommented to match the specifications of

Leadtek GPS-9546	**uBlox LEA-4A**
HplGps9546C.nc	HplGpsUbloxLea4aC.nc
HplGps9546P.nc	HplGpsUbloxLea4aP.nc
gps9546C.nc	gpsUbloxLea4aC.nc
gps9546P.nc	gpsUbloxLea4aP.nc

Table 3.1: GPS Drivers, filename changes

```
implementation {
  atm128_uart_config_t c4800 = {//NMEA standard
    ATM128_UART_BAUD_4800,
    ATM128_UART_CLOCK_DOUBLE,
    ATM128_UART_CHARSIZE_8,
    ATM128_UART_PARITY_NONE,
    ATM128_UART_STOPBITS_1,
  };

  command error_t StdControl.start(){
    if(call UartControl.start() == SUCCESS) {
      call UartConfig.setConfig(&c4800);
      return SUCCESS;
    } else {
      return FAIL;
    }
  }
```

Table 3.2: Leadtek baud rate code

the NMEA packet sent by the uBlox module. Testing of the modified code showed that it still failed to successfully control the GPS module. This testing was performed using a slightly modified version of the TestNmeaParse application used previously to test the Leadtek driver. The application was modified so that it used the uBlox components under development, instead of the Leadtek driver components.

Further online research located a paper by Silva et al. [49], who claimed to have developed a driver for the MTS420CC sensorboard. In the paper they mention making several changes, including changing the baud rate. This change had not been attempted in our work due to the uBlox module datasheet mentioning a number of baud rates, including the baud rate originally used in the code.

The baud rate settings in the code were modified from that shown in table 3.2 to the settings shown in table 3.3. The TestNmeaParse application was then recompiled and reloaded onto a mote. The changes to the code had the desired effect and GPS coordinates were received on the PC. During testing it was noted that the figure given in the uBlox manual for a cold start is inaccurate. The manual gives 41 seconds as the maximum startup time. Re-

```
implementation {
  atm128_uart_config_t c9600 = {
    ATM128_UART_BAUD_9600,
    ATM128_UART_CLOCK_DOUBLE,
    ATM128_UART_CHARSIZE_8,
    ATM128_UART_PARITY_NONE,
    ATM128_UART_STOPBITS_1,
  };

  command error_t StdControl.start() {
    if(call UartControl.start() == SUCCESS) {
      call UartConfig.setConfig(&c9600);
      return SUCCESS;
    } else {
      return FAIL;
    }
  }
```

Table 3.3: uBlox baud rate code

peated cold starts of the mote/sensorboard combination showed that the average startup time was close to two minutes. It was also noted that the altitude reported by the GPS module varied widely on a timescale of minutes.

3.3 Measuring Altitude with a Pressure Sensor

Since the altitude returned by the uBlox GPS module was not accurate enough for use in even a demonstration system it was decided to use the Intersema MS5534 pressure sensor on the MTS420 as an altimeter [39, 50]. An altimeter makes use of the relationship between pressure and depth in a gas to calculate the height above sea level. In an incompressible fluid like water, the relationship between pressure and depth is $P = \rho g h$ where ρ is the density of the fluid and g is the acceleration due to gravity at the surface of the earth ($9.81ms^{-2}$). For mixtures of gases like air, the relationship between pressure P and height h is more complicated because the density varies as the pressure varies. The relationship is given by

$$h = cT \ln \frac{P}{P_0}$$

where P_0 is the pressure at sea level, P is the measured pressure, T is the temperature and c is a constant related to the molecular properties of the gas [37].

Given the lack of any driver for the pressure sensor, initial work on building a driver focused on understanding (a) how the pressure sensor is wired on the MTS420 sensorboard and (b) the communication protocol it expects. The MTS420 documentation [39] shows the

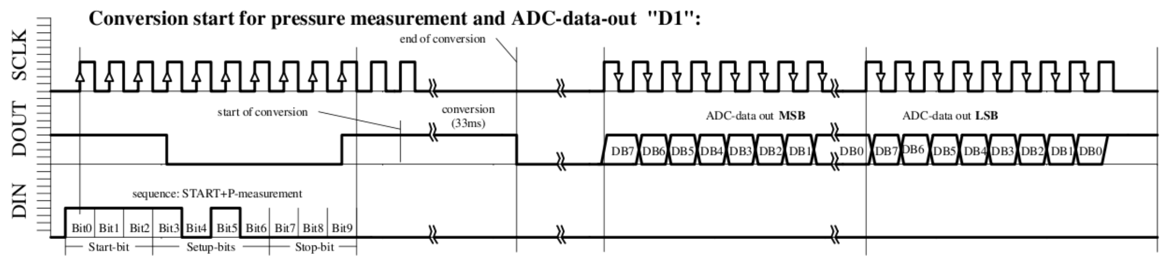

Conversion start for pressure measurement and ADC-data-out "D1":
SCLK
DOUT
DIN
end of conversion
start of conversion
conversion (33ms)
ADC-data out MSB
ADC-data out LSB
DB7 DB6 DB5 DB4 DB3 DB2 DB1 DB0 DB7 DB6 DB5 DB4 DB3 DB2 DB1 DB0
sequence: START+P-measurement
Bit0 Bit1 Bit2 Bit3 Bit4 Bit5 Bit6 Bit7 Bit8 Bit9
Start-bit
Setup-bits
Stop-bit

Figure 3.2: Pressure Acquisition Sequence *(Image reproduced from MS5534 manual [50])*

pressure sensor as being connected to the USART1 hardware interface of the MICAz mote's processor [26]. This is the same interface that the GPS sensor discussed in the last section, is connected to. A comparison of the communication protocol expected by the MS5534 pressure sensor and the capabilities of the USART1 interface revealed a fundamental incompatibility [26, 50]. The pressure sensor requires that each instruction sent to the device is followed by two further ticks of the serial clock line. This is shown in figure 3.2, which shows the timing diagram for reading the pressure from the sensor. To control the number of ticks of the clock, the ATMega128 datasheet implies that the USART hardware should be placed in a synchronous clock operation mode. (See pg. 175 of [26].) The datasheet does not make it clear, however, whether the synchronous mode will produce clock ticks only if data is being transmitted. Investigation of the TinyOS driver code for the USART system showed that it only implements the asynchronous operation mode. The imprecise information on the USART and the need to reimplement a core part of the TinyOS system led to a decision to build a demonstration system using dedicated hardware. This decision is discussed in detail in the next section, and a complete description of the hardware is covered in chapter 4.

3.4 Summary of the limitations of the Mote Prototype

A number of important limitations of mote based prototyping were identified as the work described in this chapter progressed. These limitations are:

- The frequency which the motes operate at is unlicenced and also ZigBee is a short range communication system. These factors made it ideal for building a proof of concept system. A real system, however would have to operate in a frequency band licenced to the aviation industry world wide, such as in the VOR or Secondary Surveillance Radar bands [10].
- The altitude returned by the GPS sensor is not stable enough to be useful.
- The TinyOS driver for the USART interface of the ATMega processor may have to be reimplemented, to allow reading of the pressure sensor.

Given these limitations a decision was made to build the dedicated hardware described in chapter 4.

Chapter 4

Building Dedicated Hardware

The dedicated hardware is designed to detect the frequencies used by the VOR navigation system (108-118MHz). It was decided to use these frequencies for two reasons,

1. Part of the operation of the VOR system involves it transmitting a constant signal. This signal is constant in a radius around the VOR transmitter and so would make any system detecting it omnidirectional.

2. The strength of the constant signal from the VOR station decays with distance from the station. This decay rate is proportional to $\frac{1}{r^2}$ and as such can be used to detect the distance that the detector is at from the station.

The first section of this chapter gives an overview of the functioning of the dedicated hardware. Subsequent sections describe the functioning of each component in detail and the final section describes the fully assembled hardware.

4.1 Overview

The Controlled Airspace Boundary Detector consists of three stages: an *input* stage, a *power measuring* stage and an *output* stage. The *input* stage consists of an antenna, and a filter which removes the frequencies outside the 108MHz to 118MHz range of VOR. The *power measuring* stage provides an output voltage proportional to the power of the input signal. The *output* stage signals a warning in the form of an LED when the measured signal power exceeds a predefined threshold.

4.2 Input Stage

The input stage of the Controlled Airspace Boundary Detector consists of an antenna and an A11535 crystal filter manufactured by Advanced Material Technologies [51]. Crystal filters exploit Surface Accoustic Waves (SAW) on a quartz crystal to filter incoming signals. An electrode is attached at each end of the quartz crystal. The signal at the input electrode

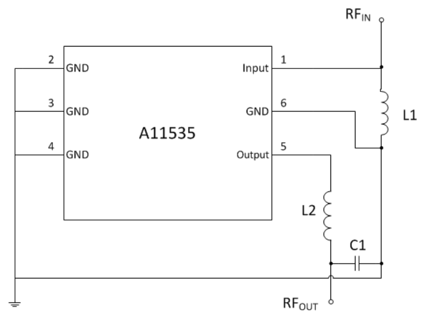

Figure 4.1: A11535 Bandpass Filter, Test Circuit

excites a SAW in the crystal, and the output electrode converts it back to an electrical signal. The geometric properties of the crystal (length, width, etc.) determine which frequencies can pass through the filter [52].

The antenna is a simple monopole antenna as described in section 2.7. It receives the VOR signal and a large number of other frequencies above and below the VOR frequency band. The A11535 filter is used to remove the frequencies outside the VOR band.

4.2.1 A11535 Bandpass Filter

The A11535 bandpass filter has a 3dB bandwidth of 4.93MHz centered at 115MHz [51]. It has a high impedance at all frequencies outside the bandwidth. This allows the VOR frequencies to pass through the filter and removes all other frequencies detected by the antenna. Figure 4.1 shows the circuit used to test the operation of the filter. An RF signal is input at the RF_{in} terminal. For testing, the input signal is generated by a signal generator. The output of the filter is measured at the RF_{out} terminal. The values of the inductors L1 and L2 are 56nH and 22nH, respectively, and the capacitor C1 is 39pF.

4.3 Power Measuring Stage, LTC5507

The power measuring stage of the detector is the core of the system. It consists of the evaluation board for the Linear Technologies LTC5507 RF Power Detector [53], [54]. The LTC5507 RF power detector consists of a Schottky diode and an amplifier integrated into a single chip [53].

A diode is an electronic component which conducts current in only one direction. A Schottky diode is a special form of diode which has a fast switching performance and the voltage drop across it is very low. Normal diodes consist of two pieces of silicon with different doping characteristics called *p* and *n* type. A Schottky diode is made from a metal joined to an *n*-type piece of silicon [55]. For power detection, a Schottky diode is used in conjunction with a capacitor. In the case of the LTC5507 this capacitor is an external component [53].

An amplifier is a device which changes the magnitude of a signal. In the LTC5507 power detector, a buffered amplifier is used. This prevents any interference between the output and

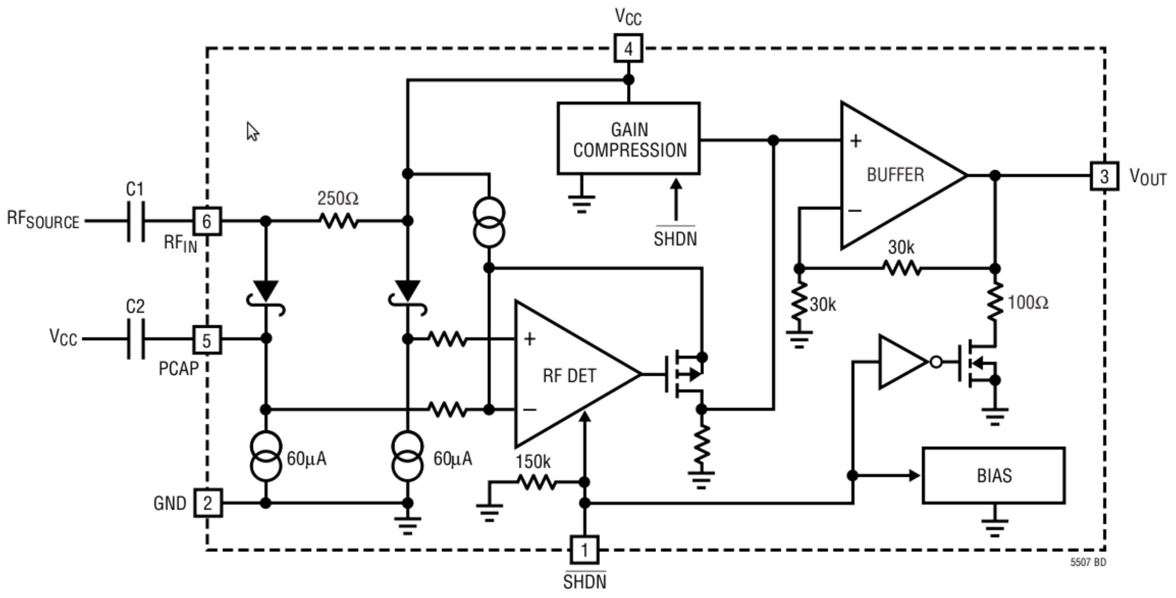

Figure 4.2: LTC5507 Internal Block Diagram *(Image reproduced from LTC5507 manual [53])*

the input.

Figure 4.2 shows a block diagram of the internal components of the LTC5507 power detector chip. The RF input is connected to the Schottky diodes on the left of the image. Output from the detector stage is fed into the buffered amplifier on the right of the image, which is connected to the V_{out} pin.

4.3.1 Testing of the LTC5507 Evaluation Board

Initial testing of the LTC5507 Evaluation Board was done to verify the accuracy of the output range claimed in the datasheet [53], and to find the input voltage needed to give the maximum output. The evaluation board circuit diagram is shown in figure 4.3. The demo board's external connections are labeled E1 through E5, and J1. RF signals are supplied to the board through a co-axial connector at J1. The power supply to the chip is connected between V_{CC} and GND at E1 and E3. The output voltage is measured between V_{out} (E2) and GND.

For the initial testing of the LTC5507 demo board, a signal generator was used to supply the RF signal. This signal generator has a maximum peak-to-peak output of 21.4V, which exceeds the maximum specifications of the LTC5507 chip. A potential divider is therefore used to limit the maximum voltage. A typical experimental setup is shown in figure 4.4. The output of the signal generator is connected to a potential divider. The RF input of the LTC5507 is connected via a co-axial cable to the V_{out} of the potential divider and the negative of the signal generator (not shown). The LTC5507 is powered by a direct current (DC) power supply set to 5.5 volts and connected between E1 and E3. The output of the LTC5507 chip was measured using an oscilloscope between terminals E2 and E3 of the demo board.

A series of tests were carried out with the voltage supplied to the RF input pin of the LTC5507 being increased each time. The results of this series of tests is shown in table 4.1. From the table, the input impedance can be calculated as follows. The output voltage can

R1 $\Omega \pm 5\%$	**R2** $\Omega \pm 5\%$	**Potential Divider** Vout $\pm 0.1V$	**LTC5507** Vout $\pm 0.02V$	**Power** dBm± 1	**Impedance** $\Omega \pm 100$
560	68	2.2	1.05	3	2400
390	68	2.8	1.25	5	1900
180	68	4.8	1.95	12	1500
120	68	5.8	2.25	13	1300

Table 4.1: LTC5507 Tests. 2 MHz

R1 $\Omega \pm 5\%$	**R2** $\Omega \pm 5\%$	**Potential Divider** Vout $\pm 0.1V$	**LTC5507** Vout $\pm 0.02V$	**Power** dBm± 1	**Impedance** $\Omega \pm 1000$
560	68	2.2	0.70	-4	12000
390	68	2.8	0.76	-2	12000
180	68	4.8	0.92	1	18000
120	68	5.8	1.10	3	17000

Table 4.2: LTC5507 Tests. 200 KHz

be converted to input power using the graphs in the LTC5507 datasheet [53]. Taking the final output voltage of 2.25 volts, and using the datasheet, the input power is found to be $\sim$ 13dBm. Using the input voltage of 5.8V, equation 2.4, and converting 13dBm to 20mW, gives an input impedance of $\sim$ 1300Ω.

Tables 4.1 and 4.2 show the results of testing the LTC5507 chip at 2MHz and 200kHz, respectively. It can be seen that the impedance of the chip is an order of magnitude higher at the lower frequency. The variation in input impedance with frequency means that the potential divider must be changed to achieve the same input power at different frequencies. As the frequency decreases, the input RF voltage must be increased to maintain the same measured power level by the LTC5507 chip.

4.4 Output Stage

The output stage of the Controlled Airspace Boundary Detector consists of an AZV393 dual voltage comparator manufactured by BCD Semiconductor, and an LED [56]. The purpose of the output stage is to convert the measurements performed by the power measuring stage into a simple visual indicator of an LED lighting, or not lighting, depending on the presence

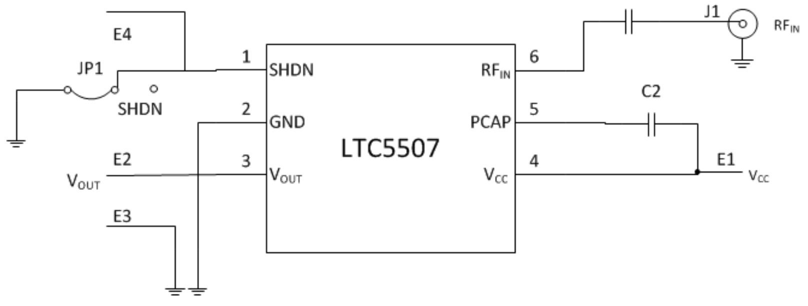

Figure 4.3: LTC5507 Evaluation Board Circuit Diagram

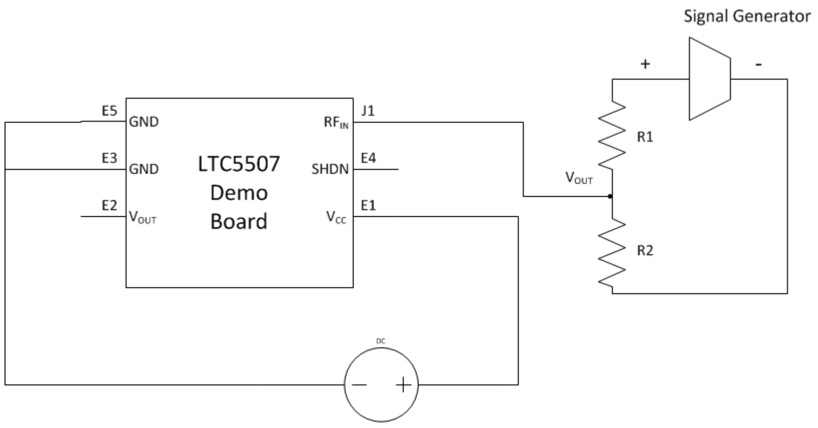

Figure 4.4: LTC5507 Test Circuit Diagram

In -	In +	Output
$<$	V_{ref}	high
$>$	V_{ref}	low
V_{ref}	$<$	low
V_{ref}	$>$	high
V_{ref}	Unconnected	high
Unconnected	Unconnected	low

Table 4.3: Voltage Comparator Truth Table

or absence of a signal.

4.4.1 Testing of the AZV393 Voltage Comparator

The AZV393 chip contains two independent voltage comparators, only one of which is used in the Controlled Airspace Boundary Detector. Figure 4.5 shows the test circuit for the AZV393 chip. The power supply is connected between V_{cc} (pin 8) and GND (pin 4). The reference voltage is connected to In- (pin 2) and the test voltage to In+ (pin 3). The output of the voltage comparator is measured between V_{out} (pin 1) and GND (pin 4).

The function of the voltage comparator is to compare the input voltage on two wires, In+ and In-. If the voltage on the two wires differs, then the output of the voltage comparator switches. Table 4.3 shows the range of possible values for the output voltage. The symbols $<$ or $>$ mean the voltage on a pin is less or greater than the reference voltage V_{ref}. *Unconnected* means that no input was connected to the pin. Low means 0V and high means the voltage is equal to V_{CC}.

Lines 3 and 4 of table 4.3 are the section of the truth table in use in the Controlled Airspace Boundary Detector. The reference voltage is connected to In- and the test voltage is connected to In+. When the test voltage is less than V_{ref}, the output of the voltage comparator is low. When the test voltage exceeds V_{ref}, the output of the comparator is high.

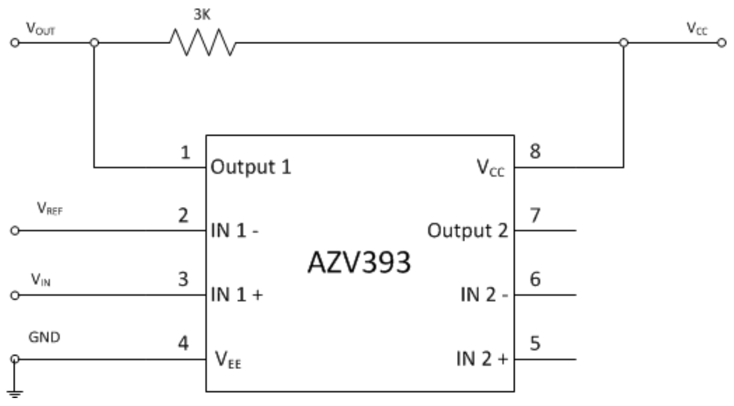

Figure 4.5: AZV393 Test Circuit Diagram

4.5 Overview of the Fully Assembled System

In the controlled airspace boundary detector circuit, the input, power measuring and output stages are connected together as shown in figure 4.6. The RF output of the input filter is connected to the RF input (J1) of the LTC5507 demo board. The output of the LTC demo board at terminal E2 is connected to the In+ of the AZV393 voltage comparator. The reference voltage to the In- input of the voltage comparator is supplied from the output of the potential divider formed by R1 and R2. An LED is connected between the ouput pin of the voltage comparator and ground. Chapter 5 discusses the testing of the system, including the configuration of the detection threshold.

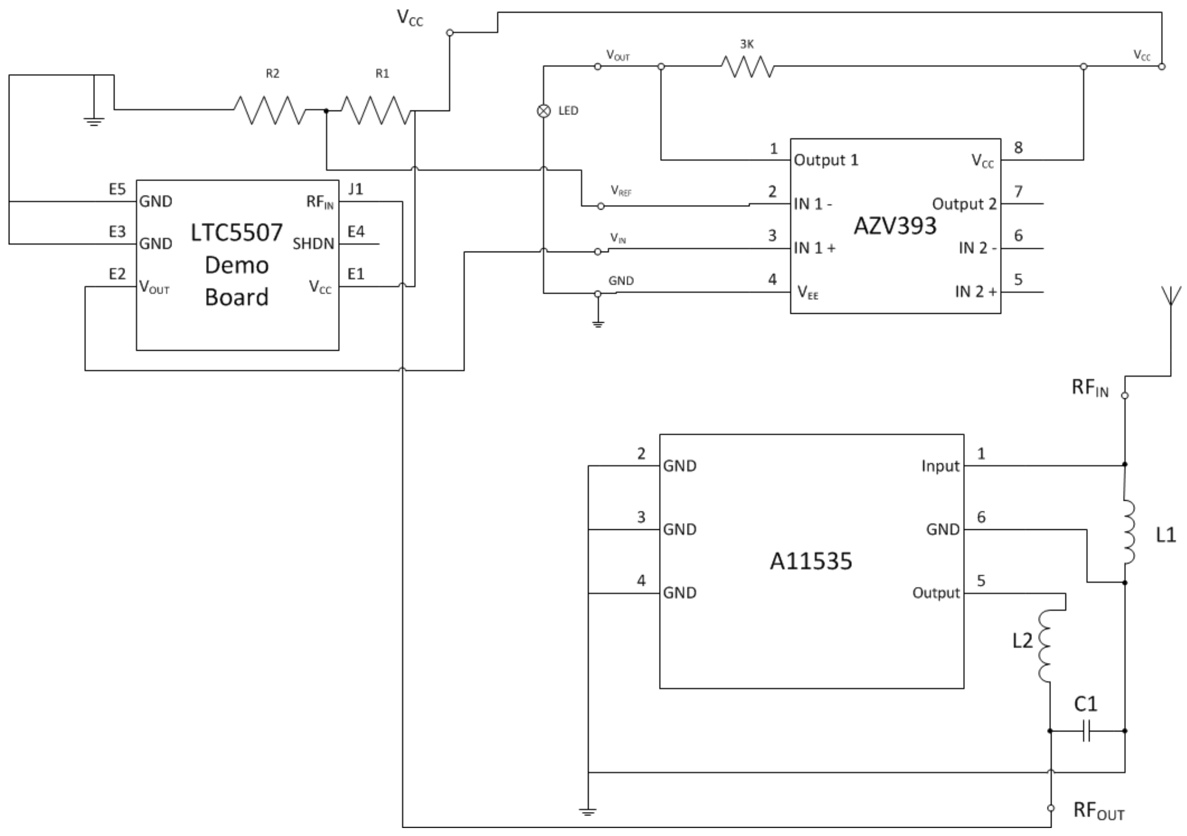

Figure 4.6: Controlled Airspace Boundary Detector Circuit

Chapter 5

Results and Analysis

This chapter discusses the testing of the detector circuit and the selection of a detection threshold based on those tests.

5.1 Overview

The detector circuit shown in figure 4.6 needs to be configured so that it will only light the warning LED when a real signal is detected. This configuration is accomplished in two stages. First, the output of the combined input and power metering stages must be measured while a signal is being input at different frequencies. The results of these tests must be used to decide on an appropriate reference voltage for the voltage comparator of the output stage.

5.2 Testing the Input and Power Measuring Stages

To test the input and power measuring stages, a signal generator was connected to the RF input of the filter, instead of the antenna shown in figure 4.6. The output from the LTC5507 demo board was directly measured using an oscilloscope. The signal generator was set to different frequencies and the output of the LTC5507 demo board was recorded at each frequency. The frequencies ranged from below the passband of the A11535 filter to above the passband [51]. Table 5.1 shows the results of these tests. The output values for 108MHz and 118MHz (the edges of the VOR band) are 300mV and 440mV, respectively. It was decided that the reference voltage supplied to the voltage comparator should therefore be greater than 440mV. A value of 445mV was chosen to ensure that only signals from the VOR frequency range would trigger the detector.

5.3 Configuring the Detection Threshold

Choosing a detection threshold required selecting values for resistors R1 and R2 in the potential divider in figure 4.6. A 10kΩ resistor was chosen for R1. The value of R2 was calculated

Input Frequency MHz	**Output Voltage** mV
100	290
103	290
106	290
108	300
109	310
112	380
115	460
118	440
121	400
124	380
127	360
130	340

Table 5.1: Input and Power Measuring stage test results at 0dBm

using equation 2.5. The power supply voltage (5V), is V_{IN}. V_{OUT} is 445mV for the reasons discussed in the previous section. The value calculated for R2 was 976Ω, therefore a 1kΩ resistor was used as R2. The output of the potential divider was then connected as the reference voltage to the AZV393 voltage comparator.

Testing of the circuit with this combination of resistors revealed that it falsely detected frequencies as high as 125MHz. The value of R2 was increased in 50Ω steps, until the circuit only responded to frequencies within the VOR range. The final value of R2 was 1.2kΩ, which corresponds to a potential divider output/reference voltage of 536mV.

5.4 Final Testing

The final reference voltage of 536mV is clearly greater than the peak output voltage of 460mV at 115MHz in table 5.1. This inconsistency was investigated, by measuring the output voltage of the power measuring stage while it was connected to the voltage comparator. The frequency was swept from 100MHz to 130MHz in increments of 3MHz and the output measured at each step. It was observed during these tests that the output of the circuit fluctuated, depending on the relative positions of the various co-axial cables and the oscilloscope probes. It was theorized based on this behaviour that interference existed between various parts of the circuit.

Two possible causes for the interference were identified: (a) that the input cable from the signal generator and the output cable from the filter were interfering with each other, and (b) that the use of two ground rails (joined with a length of wire) on the breadboard was acting as an antenna. Figure B.2 shows a picture of the breadboard at the conclusion of the project, with the ground rails labeled. Due to the time constraints of the project, further testing to find and eliminate the source of the interference was not possible.

Chapter 6

Evaluation and Future Work

This chapter evaluates the Controlled Airspace Boundary Detection project with respect to the goals outlined in section 1.2. It also outlines some possible future work which would improve and extend the detector.

6.1 Evaluation

The primary goal of this project was to produce a detector capable of providing a pilot with adequate warning of controlled airspace ahead. With respect to this goal, the final circuit is reasonably successful. It can detect frequencies in the VOR frequency band and display a warning in the form of a lighted LED.

There are also some issues with the final circuit, including:

- Self interference
- Overly restricted bandwidth
- Unknown detection range and limited sensitivity.

The problem of self interference, as outlined in the final section of chapter 5, is the most serious. This self interference could be reduced in a number of ways, firstly, a replacement for the LTC5507 RF power meter, suitable for use on a breadboard, could be found. This would eliminate the co-axial cable from the input stage components to the LTC5507 demo board. Secondly, the components could be rearranged on the breadboard so that only one ground rail would be utilised. Finally, the rearrangement of the components should be done in a way that minimised the length of all wires on the breadboard. This would help to reduce the potential of each wire to act as an unwanted antenna.

The bandwidth restriction is caused by the A11535 filter. which supresses all VOR frequencies outside it's 112.5MHz to 117.5MHz passband. This problem could be solved by locating and installing, a filter with a 10MHz bandwidth centered at 113MHz, the exact center of the VOR band.

The detection range of the circuit, can only be determined by experiment. The output power of a VOR transmitter would need to be measured. Then the RF power at the controlled airspace boundary would have to be either (a) measured, or (b) calculated from the transmitter power. The RF power at the desired range could be used in the configuration phase (described in chapter 5) to decide on a suitable detection threshold.

The limited sensitivity of the circuit, is partly caused (i) by the LTC5507 chip having a lower power detection threshold of -34dBm, and (ii) by losses in the A11535 filter, which reduce the signal power reaching the power measuring stage.

6.2 Future Work

In light of the recent commercial release of the *Aware* GPS system (a GPS-based navigation system that uses a built-in map to provide warnings of controlled airspace [57]), one possible avenue of future work is to enhance our system to recognise and handle real-time updates to controlled airspace. For example, the Controlled Airspace Boundary Detector could be redesigned to receive notifications of updated airspace boundaries from an airport. It could then incorporate these changes into the *Aware* system's on-board map. Such a real-time updating of the controlled airspace would prevent pilots accidentally infringing newly controlled airspace.

Appendix A

Code Listings

A.1 Blink Demonstration Application

A.1.1 Blink Configuration Code

```
configuration BlinkAppC
{
}
implementation
{
  components MainC, BlinkC, LedsC;
  components new TimerMilliC() as Timer0;

  BlinkC -> MainC.Boot;

  BlinkC.Timer0 -> Timer0;
  BlinkC.Leds -> LedsC;
}
```

A.1.2 Blink Module Code

```
#include "Timer.h"

module BlinkC @safe()
{
  uses interface Timer<TMilli> as Timer0;
  uses interface Leds;
  uses interface Boot;
}
implementation
{
  event void Boot.booted()
  {
    call Timer0.startPeriodic( 250 );
  }

  event void Timer0.fired()
  {
    dbg("BlinkC","Timer 0 fired @ %s.\n", sim_time_string());
    call Leds.led0Toggle();
  }
}
```

A.2 ReadRSSI Version One Code

A.2.1 ReadRSSI Configuration Code

```
#include "printf.h"

configuration RssiAppC
{
}
implementation
{
  components MainC, RssiC, LedsC;
  components new TimerMilliC() as Timer0;
  components CC2420ControlC;
  components HplCC2420InterruptsC;
//  components new CC2420SpiC();
//  components new AMReceiverC(6) as Receiver;

  RssiC -> MainC.Boot;

  RssiC.Timer0 -> Timer0;
  RssiC.Leds -> LedsC;
  RssiC.Read -> CC2420ControlC.ReadRssi;
  RssiC.Resource -> CC2420ControlC.Resource;
  RssiC.Config -> CC2420ControlC.CC2420Config;
  RssiC.Power -> CC2420ControlC.CC2420Power;
  RssiC.Sfd -> HplCC2420InterruptsC.CaptureSFD;
  RssiC.Cca -> HplCC2420InterruptsC.InterruptCCA;
  RssiC.Fifo -> HplCC2420InterruptsC.InterruptFIFOP;
//  RssiC.ReadRxFiFo -> CC2420SpiC.RXFIFO;
//  RssiC.ClearRxFifo -> CC2420SpiC.SFLUSHRX;
//  RssiC.Receive -> Receiver;
}
```

A.2.2 ReadRSSI Module Code

```
#include "Timer.h"
#include "printf.h"

module RssiC @safe()
{
  uses interface Timer<TMilli> as Timer0;
  uses interface Leds;
  uses interface Boot;
  uses interface Read<uint16_t>;
  uses interface CC2420Config as Config;
  uses interface CC2420Power as Power;
  uses interface Resource;
  uses interface GpioCapture as Sfd;
  uses interface GpioInterrupt as Cca;
  uses interface GpioInterrupt as Fifo;
//  uses interface Receive;
//  uses interface CC2420Fifo as ReadRxFiFo;
//  uses interface CC2420Strobe as ClearRxFifo;
}
implementation
{
  enum {
    STATE_OFF = 1,
    STATE_STARTING = 2,
    STATE_STARTED = 3
  };

//  uint16_t i = 0;
  uint8_t ctr = 0;
  uint8_t dummy_data = 0;
  uint8_t state = STATE_OFF;

  event void Boot.booted()
  {
    //Start the timer
    call Timer0.startPeriodic( 500 );
//    call Timer0.startOneShot(1000);

    //Switch on the radio chip.
    call Power.startVReg();
    atomic
    {
      state = STATE_STARTING;
    }
  }

  event void Timer0.fired()
  {
    ctr++;
    printf("%d", ctr);
    printfflush();

    //Check if the radio has started and read RSSI if it has.
    atomic
    {
      if (state == STATE_STARTED)
      {
        //call ReadRxFiFo.beginRead(&dummy_data, 1);
        //call ClearRxFifo.strobe();
        //call ClearRxFifo.strobe();
        call Read.read();
      }
    }

    call Leds.set(ctr);
  }

// Events of the CC2420ControC module
  async event void Power.startVRegDone() {
    //printf("startVregDone");
    //printfflush();
    call Resource.request();
  }
  event void Resource.granted()
  {
    printf("resource granted event, starting oscillator");
    printfflush();
    call Power.startOscillator();
  }

  async event void Power.startOscillatorDone()
  {
    //printf("start osc done");
    //printfflush();
    call Fifo.enableFallingEdge();
    call Sfd.captureRisingEdge();
    call Power.rxOn();

    call Resource.release();

//    call Config.setAddressRecognition(FALSE, FALSE);
    //Change state to started
    atomic
    {
      state = STATE_STARTED;
    }
  }

  event void Config.syncDone(error_t error)
  {
    printf("sync done");
    printfflush();
  }

  event void Read.readDone(error_t result, uint16_t val)
  {
    if ( result == SUCCESS )
    {
      printf("\t\t%d\n", val);
    }
    else
    {
      printf("failed to read rssi\n");
    }
    printfflush();
  }

// Events from HplCC2420InterruptsC
  async event void Sfd.captured(uint16_t time)
  {
  }

  async event void Cca.fired()
  {
  }

  async event void Fifo.fired()
  {
  }

  //Events from the RXFIFO
//  async event void ReadRxFiFo.readDone(uint8_t *data,
//                        uint8_t length, error_t error)
//  {
//  }

//  async event void ReadRxFiFo.writeDone(uint8_t *data,
//                        uint8_t length, error_t error)
//  {
//  }

  //Receiver events
//  event message_t* Receive.receive(message_t* msg,
//                         void* payload, uint8_t len) {
//    printf("hello \n");
//    printfflush();
//    return msg;
//  }
}
```

A.3 ReadRSSI Version Two Code

A.3.1 ReadRSSI Configuration Code V2

```
#include "printf.h"

configuration RssiAppC
{
}
implementation
{
  components MainC, RssiC, LedsC;
  components new TimerMilliC() as Timer0;
  components CC2420ControlC;
  components ActiveMessageC;

  RssiC -> MainC.Boot;
  RssiC.Timer0 -> Timer0;
  RssiC.Leds -> LedsC;
  RssiC.Read -> CC2420ControlC.ReadRssi;
  RssiC.AMControl -> ActiveMessageC;
  RssiC.Config -> CC2420ControlC.CC2420Config;
}
```

A.3.2 ReadRSSI Module Code V2

```
#include "Timer.h"
#include "printf.h"

module RssiC @safe()
{
  uses interface Timer<TMilli> as Timer0;
  uses interface Leds;
  uses interface Boot;
  uses interface Read<uint16_t>;
  uses interface CC2420Config as Config;
  uses interface SplitControl as AMControl;
}
implementation
{
  enum {
```

```
  STATE_OFF = 1,
  STATE_STARTING = 2,
  STATE_STARTED = 3
};

uint8_t ctr = 0;
uint8_t dummy_data = 0;
uint8_t state = STATE_OFF;

event void Boot.booted()
{
  //Switch on the radio chip.
  call AMControl.start();
}

event void AMControl.startDone(error_t err)
{
 if (err == SUCCESS)
  {
    atomic
    {
      state = STATE_STARTED;
    }
    //Start the timer
    call Timer0.startPeriodic( 50  );
  }
  else
  {
    call AMControl.start();
  }
}

event void Timer0.fired()
{
  ctr++;
  printf("%d", ctr);
  printfflush();

  //Check if the radio has started and read RSSI if it has.
  atomic
```

```
    {
      if (state == STATE_STARTED)
      {
        call Read.read();
      }
    }
    call Leds.set(ctr);
  }

  event void Read.readDone(error_t result, uint16_t val)
  {
    if ( result == SUCCESS )
    {
      printf("\t\t%d\n", val);
    }
    else
    {
      printf("failed to read rssi\n");
    }
    printfflush();
  }

  event void AMControl.stopDone(error_t err)
  {
  }

  event void Config.syncDone(error_t error){
  }
}
```

A.4 Task-based ReadRSSI module code

```
#include "Timer.h"
#include "printf.h"

module RssiC @safe()
{
  uses interface Leds;
  uses interface Boot;
  uses interface Read<uint16_t>;
  uses interface CC2420Config as Config;
  uses interface SplitControl as AMControl;
}

implementation
{
  //Global variables
  enum {
    STATE_OFF = 1,
    STATE_STARTING = 2,
    STATE_STARTED = 3
  };

  uint8_t ctr = 0;
  uint8_t state = STATE_OFF;

  //Task declaration
  task void readRssiTask();

  event void Boot.booted()
  {
    //Switch on the radio chip.
    call AMControl.start();
    state = STATE_STARTING;
  }

  event void AMControl.startDone(error_t err)
  {
   if (err == SUCCESS)
    {
      state = STATE_STARTED;
      //Radio is started so post the read rssi task.
      post readRssiTask();
    }
    else
    {
      call AMControl.start();
    }
  }
  task void readRssiTask()
  {
    ctr++;
    //Check if the radio has started and post
    //readRSSITask if it has.
    if (state == STATE_STARTED)
    {
      if (call Read.read() != SUCCESS)
      {
        post readRssiTask();
      }
    }
  }

  event void Read.readDone(error_t result, uint16_t val)
  {
    if ( result == SUCCESS )
    {
      if (val > 80)
      {
        printf("%d\n", val);
        call Leds.set(ctr);
      }
    }
    else
    {
      printf("failed to read rssi\n");
    }
    printfflush();

    post readRssiTask();
  }

  event void AMControl.stopDone(error_t err){
  }

  event void Config.syncDone(error_t error){
  }
}
```

Appendix B

Miscellaneous

B.1 Conversion chart from dBm to W

dBm	mW
15	32
5	3.2
0	1
-10	0.1
-85	3.2×10^{-9}
-95	3.2×10^{-10}
-100	1×10^{-10}

Table B.1: dBm to mW conversion chart

B.2 TinyOS radio stack implementation for cc2420

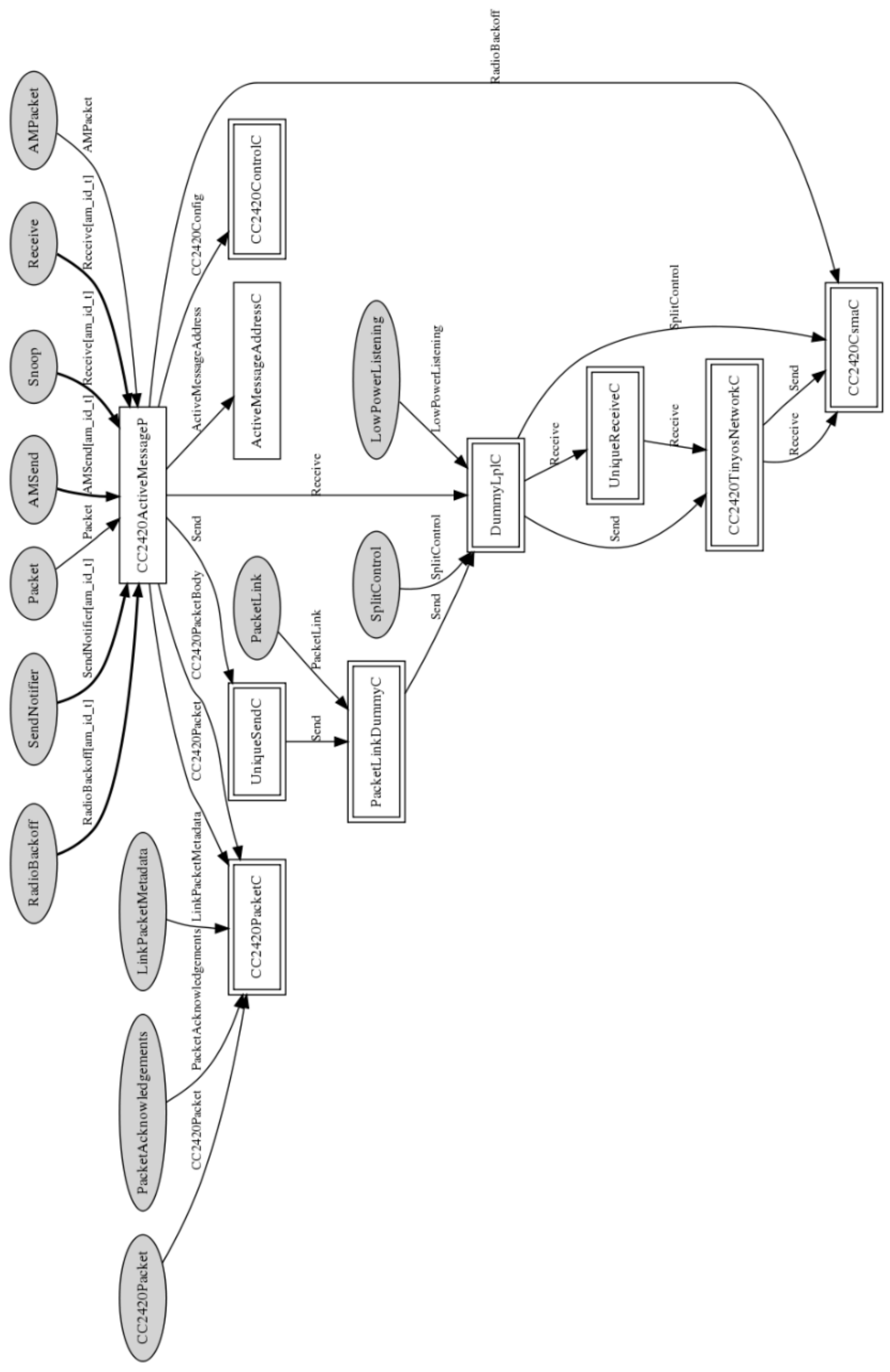

Figure B.1: TinyOS radio stack for cc2420 *(Image reproduced from CC2420ActiveMessageC documentation [58])*

B.3 Controlled Airspace Boundary Detector Prototype

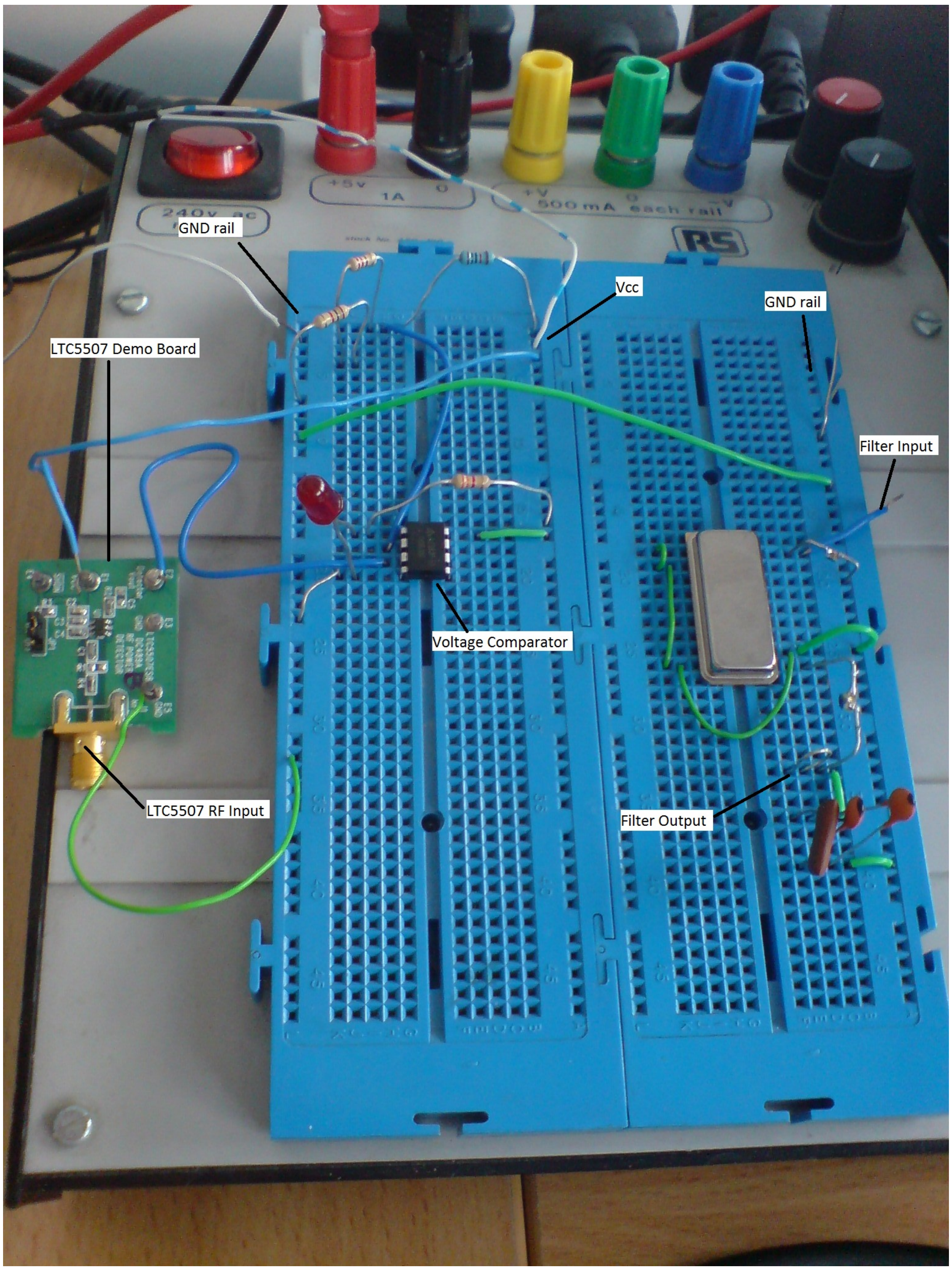

Figure B.2: Picture of the prototype on a breadboard

B.4 Listing of Lab Equipment

The following instruments were used in the development and testing of the dedicated hardware described in chapter 4.

- Thurlby Thandar Instruments (TTI) TG215 2MHz Function Generator.
- TTI EL302D Dual Power Supply
- Kenwood 40MHz Oscilloscope CS-4135
- Tektronix TDS3034 - 4 channel color digital phosphor oscilloscope 300Mhz
- Marconi Instruments 80kHz - 1040Mhz signal generator. Model 2019
- Hewlett Packard spectrum analyser 1kHz - 22GHz. Model 8562A
- Prototyping board (breadboard)

Bibliography

[1] (2010, Aug.) Annual Aviation Safety Performance Review 2009. [Online]. Available: http://www.iaa.ie/library_download.jsp?libraryID=756

[2] (2010) Occurence reporting. [Online]. Available: http://www.iaa.ie/index.jsp?p=139&n=148

[3] (2010, Aug.) Airspace Infringements Background Statistics. [Online]. Available: http://www.flyontrack.co.uk/scripts/MIAB/MIAB_ShowAsset.asp?a=-2147483622

[4] (2010, Aug.) Annual Report 2009. [Online]. Available: http://www.dublinairportauthority.com/AR_2009_English.pdf

[5] (2010, Aug.) Rules of the air, annex 2 to the convention on international civil aviation. Annex2.pdf. [Online]. Available: http://www2.tech.purdue.edu/at/courses/at300/Documents/Annex2.pdf

[6] (2010) The ICAO website. [Online]. Available: http://www.icao.int/

[7] (2010, Aug.) ENR 1.4 ATS Airspace Classifications. EI_ENR_1_4_en.pdf. [Online]. Available: http://www.iaa.ie/safe_reg/iaip/Published%20Files/AIP%20Files/ENR/EI_ENR_1_4_en.pdf

[8] (2010) How atc works? [Online]. Available: http://www.iaa.ie/index.jsp?n=248&p=153

[9] (2010) Air traffic services & technology. [Online]. Available: http://www.iaa.ie/index.jsp?p=153&n=247

[10] (2010, Aug.) Comreg radio frequency plan for ireland. ComReg0477R_39076827.pdf. [Online]. Available: http://www.comreg.ie/_fileupload/publications/ComReg0477R_39076827.pdf

[11] (2010) Air traffic services & technology. [Online]. Available: http://www.iaa.ie/index.jsp?p=155&n=255

[12] (2010) Surveillance / radar. [Online]. Available: http://www.iaa.ie/index.jsp?p=155&n=257

[13] (2010, Aug.) Mode s technical overview. [Online]. Available: http://www.eurocontrol.int/msa/public/standard_page/modes_tech_overview.html

[14] (2010, Aug.) Mode s technology. [Online]. Available: http://mit.edu/6.933/www/Fall2000/mode-s/technology.html

[15] (2010) Navigation. [Online]. Available: http://www.iaa.ie/index.jsp?p=155&n=256

[16] (2010, Aug.) Operational notes on vhf omni range VOR. [Online]. Available: http://www.casa.gov.au/wcmswr/_assets/main/pilots/download/vor.pdf

[17] (2010, Aug.) 2001 federal radio navigation systems. FRS2001.pdf. [Online]. Available: http://www.navcen.uscg.gov/pdf/frp/frp2001/frs2001.pdf

[18] (2010, Aug.) AIP Ireland, EIDW AD 2 - 1. [Online]. Available: http://www.iaa.ie/safe_reg/iaip/Published%20Files/AIP%20Files/AD/EI_AD_2_EIDW_en.pdf

[19] (2010) Crossbow website. [Online]. Available: http://www.xbow.com/

[20] (2010, Aug.) MICAz 2.4ghz wireless module. [Online]. Available: http://memsic.com/products/wireless-sensor-networks/wireless-modules.html

[21] (2010, Aug.) MPR-MIB Users Manual. Revision A, June 2007. MEMSIC. PN: 7430-0021-08. [Online]. Available: http://memsic.com/support/documentation/wireless-sensor-networks/category/6-user-manuals.html?download=61%3Ampr-mib-wireless-module-user-s-manual

[22] (2010, Aug.) Chipcon cc2420 2.4 GHz IEEE 802.15.4 ZigBee-ready RF Transceiver. Rev B, 20 Mar 2007. Texas Instruments. SWRS041B. [Online]. Available: http://www.ti.com/lit/gpn/cc2420

[23] W. Su and M. Alzaghal, "Channel propagation characteristics of wireless micaz sensor nodes," *Ad Hoc Netw.*, vol. 7, no. 6, pp. 1183–1193, 2009.

[24] (2010) Part 15.4: Wireless Medium Access Control(MAC) and Physical Layer(PHY) Specifications for Low-Rate Wireless Personal Area Networks (WPANs). [Online]. Available: http://standards.ieee.org/getieee802/download/802.15.4-2006.pdf

[25] K. Srinivasan and P. Levis, "Rssi is under appreciated," in *In Proceedings of the Third Workshop on Embedded Networked Sensors (EmNets)*, 2006.

[26] (2010, Mar.) ATmega128 AVR 8-bit Microcontroller with 128K Bytes In-System Programmable Flash. Rev. 2467SAVR07/09. Atmel. [Online]. Available: http://www.atmel.com/dyn/resources/prod_documents/doc2467.pdf

[27] (2010) Sensor boards. MEMSIC. [Online]. Available: http://memsic.com/products/wireless-sensor-networks/sensor-boards.html

[28] P. Baronti, P. Pillai, V. Chook, S. Chessa, A. Gotta, and Y. Hu, "Wireless sensor networks: A survey on the state of the art and the 802.15. 4 and ZigBee standards," *Computer Communications*, vol. 30, no. 7, pp. 1655–1695, 2007.

[29] Z. Alliance, "Zigbee-2006 specification," *ZigBee Alliance*, 2006.

[30] (2010, Aug.) TinyOS Community Forum. [Online]. Available: http://www.tinyos.net/

[31] P. Levis and D. Gay, *TinyOS Programming*, 1st ed. Cambridge University Press, 2009.

[32] (2010, Mar.) Getting Started with TinyOS. [Online]. Available: http://docs.tinyos.net/index.php/Getting_Started_with_TinyOS

[33] (2010, Aug.) Modules and the TinyOS Execution Model. [Online]. Available: http://docs.tinyos.net/index.php/Modules_and_the_TinyOS_Execution_Model

[34] (2010, Aug.) United States Updates Global Positioning System Technology. [Online]. Available: http://www.america.gov/st/washfile-english/2006/February/20060203125928lcnirellep0.5061609.html

[35] (2010, Aug.) Global Positioning System. [Online]. Available: http://www.gps.gov/systems/gps/index.html

[36] (2010, Aug.) The Global Positioning System. [Online]. Available: http://www.colorado.edu/geography/gcraft/notes/gps/gps_f.html

[37] M. Mansfield and C. O'Sullivan, *Understanding Physics*. John Wiley & Sons, 1999.

[38] S. R. Saunders, *Antennas and Propagation for Wireless Communication Systems*. John Wiley & Sons, 2004.

[39] (2010, Aug.) MTS/MDA Sensor Board Users Manual. Revision A, June 2007. MEMSIC. PN: 7430-0020-05. [Online]. Available: http://memsic.com/support/documentation/wireless-sensor-networks/category/6-user-manuals.html?download=62%3Amts-mda-sensor-board-user-s-manual

[40] (2010, Aug.) TinyOS Tutorials. [Online]. Available: http://docs.tinyos.net/index.php/TinyOS_Tutorials

[41] (2010, Aug.) TEP's. [Online]. Available: http://docs.tinyos.net/index.php/TEPs

[42] (2010, Aug.) RSSI demo. [Online]. Available: http://docs.tinyos.net/index.php/Rssi_Demo

[43] (2010, Aug.) The TinyOS printf Library. [Online]. Available: http://docs.tinyos.net/index.php/The_TinyOS_printf_Library

[44] (2010, Aug.) LEA-4A ANTARIS® 4 GPS Modules. Dec 2006. GPS.G4-MS4-06143-1. [Online]. Available: http://www.u-blox.com/images/downloads/Product_Docs/LEA-4x_Data_Sheet%28GPS.G4-MS4-06143%29.pdf

[45] (2010, Aug.) MTS420. [Online]. Available: http://docs.tinyos.net/index.php/MTS400

[46] (2010, Aug.) SourceForge.net Repository - [TinyOS] Index of /tinyos-2.x-contrib/rincon. [Online]. Available: http://tinyos.cvs.sourceforge.net/viewvc/tinyos/tinyos-2.x-contrib/rincon/

[47] (2010, Aug.) Leadtek. [Online]. Available: http://www.leadtek.com.tw/downloads/?lang=eng&filepath=/gps/9546/&filename=9546Manual%5FV1%2E12%5F20030806%2Epdf

[48] (2010, Aug.) National Marine Electronics Association. [Online]. Available: http://www.nmea.org/content/nmea_standards/nmea_083_v_400.asp

[49] R. Silva, J. S. Silva, C. Geyer, V. Leithard, and F. Boavida, "Use of gps and 6lowpan in mobile multi-sink wireless sensor networks - issues and feasibility," in *8th International Information and telecommunication Technologies Symposium (I2TS)*, Dec. 2009, pp. 154–160, ISBN 978-85-8.

[50] (2010, Aug.) MS5534C Altimeter/Barometer Module. [Online]. Available: http://www.intersema.ch/index.php?option=com_rubberdoc&view=doc&id=35&format=raw

[51] (2010, Aug.) 115MHz Bandpass Filter 4.92MHz Bandwidth. [Online]. Available: http://www.amtsaw.com/brochure/saw/A11535.pdf

[52] E. Benes, M. Groschl, F. Seifert, and A. Pohl, "Comparison between BAW and SAW sensor principles," in *Frequency Control Symposium., Proceedings of the 1997 IEEE International*, may. 1997, pp. 5 –20.

[53] (2010, Aug.) LTC5507 - 100kHz to 1GHz RF Power Detector. [Online]. Available: http://cds.linear.com/docs/Datasheet/5507f.pdf

[54] (2010, Aug.) DC489 - LTC5507 Evaluation Kit. [Online]. Available: http://cds.linear.com/docs/Reference%20Design/dc489A.pdf

[55] M. J. Cooke, *Semiconductor devices.* Prentice-Hall, Inc. Upper Saddle River, NJ, USA, 1990.

[56] (2010, Aug.) Dual General Purpose Low Voltage Comparator, AZV393. [Online]. Available: http://www.bcdsemi.com/upload/datasheet/AZV393%20D1.3%20091117.pdf

[57] (2010, Sep.) The Aware Airspace Alerting Tool. [Online]. Available: http://www.airspaceaware.com/aboutaware/

[58] (2010, Aug.) Interfaces and Components. [Online]. Available: http://www.tinyos.net/tinyos-2.x/doc/nesdoc/micaz/index.html